Colloid Polym Sci (2008) 286:159–168
DOI 10.1007/s00396-007-1759-9

ORIGINAL CONTRIBUTION

Self-assembled ultra-thin coatings of octadecyltrichlorosilane (OTS) formed at the surface of iron oxide nanoparticles

Patrick Degen · Anuj Shukla · Uwe Boetcher · Heinz Rehage

Received: 11 July 2007 / Revised: 8 August 2007 / Accepted: 8 August 2007 / Published online: 5 September 2007

Abstract In a series of experiments, we coated iron oxide nanoparticles, which were originally stabilized with lauric acid, with a polymer layer of Octadecyltrichlorosilane (OTS). Characterization of the different coated nanoparticles was accomplished by Static and Dynamic Light Scattering, acoustic spectroscopy, and Atomic Force Microscopy. In various experiments, we systematically investigated the effect of different parameters such as the OTS concentration and iron oxide content on the particle size of the coated nanoparticles. It was recognized that the size of the coated nanoparticles mainly depend on the concentration of OTS (C_{OTS}) measured with respect to the concentration of the iron oxide particles ($C_{mag.}$). Below a well-defined threshold value of C_{OTS}/C_{mag}, we did not observe any adsorption of OTS on the surface of iron oxide nanoparticles. The particle size of OTS-coated iron oxide nanoparticles increased rapidly at concentration ratios above the threshold concentration and reached a typical plateau value for long periods of time.

Keywords Magnetic nanoparticles · Octadecyltrichlorosilan · Polysiloxane · Nanocapsules

Introduction

Nowadays, synthesis and study of nanometer-size particles are the subjects of intense research activities [1]. Reduction of the particle size to the nanometer scale leads to a quantitative change of physical and chemical features, and small particles obey quantum-mechanical properties. Iron oxide nanoparticles, both fine crystalline and amorphous, have many important applications in magnetic recording, solar energy transformation, magnetic fluids, electronics, and chemical catalysis [1]. To enhance stability, small particles may be coated by different organic molecules, which form a chemical bond with the molecules on the particle surface. Such materials are considered to have potential applications in biological cell dissolution, in magnetic separation of minerals as fillers in polymer matrices, and also for the removal of toxic elements from industrial wastes [1]. If the molecules surrounding the particles are able to react with each other, it is possible to synthesize ultra-thin, cross-linked networks around the nanoparticles. This leads to the formation of capsules, which are filled with magnetic nanoparticles.

Self-assembled monolayer (SAM) of different adsorbents on solid surfaces have become one of the central themes in modern materials science [2–8], and molecular level engineering of stable model surfaces has been accomplished using SAM [9]. Fewer publications have described the synthesis and characterization of self-assembled (SA) coatings on metal or on metal oxide powders [10–12]. In all of these investigations [10–12], coated surfactants act as a stabilizer, and these layers are believed to prevent agglomeration. The general trend of these studies has been that the higher the amount of surfactant, the smaller the resulting particle size [10–12], Rozenfeld et al. [12] synthesized Octadecyltrichlorosilane (OTS)-coated particles and found lower stabilization than obtained with Sodium Dodecyl Sulfate. We have recently studied the coating of OTS on the magnetic particle synthesized in reverse micellar cavity [13] In this study, iron oxide nanoparticles stabilized by

P. Degen (✉) · A. Shukla · U. Boetcher · H. Rehage
Lehrstuhl für Physikalische Chemie II, Universität Dortmund,
Otto-Hahn-Str. 6,
44227 Dortmund, Germany
e-mail: patrick.degen@uni-dortmund.de

H. Rehage
e-mail: heinz.rehage@uni-dortmund.de

lauric acid have been used as substrates for SA coating processes of OTS molecules. Up to now, there is no information about controlling the size of coated iron oxide nanoparticles just by varying the amount of OTS concentration. In a series of experiments, we systematically investigated the effect of nanoparticle and OTS concentration. It turned out that the concentration ratio, defined as $\mu = C_{OTS}/C_{mag}$, influenced the size and shape.

Static- and Dynamic Light Scattering (SLS and DLS) are powerful tools for determining small changes in the size of nanoparticles, which might for instance, be induced by the adsorption of other molecules at the surface. In the present study, the adsorption of OTS molecules at the surface of iron oxide nanoparticles changed the diffusion coefficient of these magnetic particles. The characteristic Brownian motion of the modified particles was measured by means of DLS. Additionally, we used Atomic Force Microscopy (AFM) to confirm the results of the nanoparticle sizes and the influence of the OTS molecules. Tapping mode and phase imaging techniques of AFM [14–16] were used to analyze our samples. In tapping mode of AFM, the cantilever was excited into resonance oscillations with a piezoelectric driver. The oscillation amplitude was used as a feedback signal to measure topographic variations of the sample. In phase imaging, the phase lag of the cantilever oscillation, relative to the signal sent to the cantilever's piezo driver, was simultaneously monitored by an extender electronics module. The measured phase lag was dependent on the composition of the sample. Tapping mode and phase imaging could be performed simultaneously, thereby offering topographical and compositional data for the same scan area.

We report on new efforts to understand the basic interactions between lauric acid coated iron oxide nanoparticles and the OTS molecules. SA layers provide us with the potential to engineer surface properties such as wettability, adhesion, adsorption, and template crystallization. For these potential applications, we need a complete understanding of the process dynamics and the ways to control it. The objective of this study is to monitor, in situ, the self-assembly process of OTS over long periods of time and to accurately determine the growth of size as a function of time.

Experimental section

Materials

OTS (purity 98%), lauric acid, tert-Butylmethylether (TBME, purity 99+%), p-Xylene (purity 99+%), and Chloroform (purity 99+%) were purchased from Sigma-Aldrich, Germany. Water was used in bidistilled quality.

Synthesis of coated iron oxide nanoparticles

The iron oxide cores were prepared as described by F. C. Meldrum [17]. Solutions of 3.0 g of $FeCl_3$ 4 H_2O in 12.5 ml of water and 6.0 g of $FeCl_2 \cdot 6\ H_20$ in 12.50 ml of water were combined, and 12.5 ml of ammonium hydroxide (14.8 M) was added under vigorous stirring. The resulting black precipitate of magnetite was settled by placing a magnet below the beaker, and the supernatant solution was then decanted. Afterwards, the solid was resuspended in 25.0 ml of 0.75 M ammonium hydroxide. The solid nanoparticles were then isolated again using magnetic separation and decantation. The remaining water was removed by evaporation in vacuum at room temperature. A solution of 0.40 g of lauric acid in 20.0 ml of ethanol was then subsequently added to the solid, and dispersion of the magnetite was induced by sonification. The ethanol was then removed by rotary evaporation, and the dried magnetite was resolved in 20 ml of chloroform, by sonification again. After subsequent extraction, we obtained a dry powder of magnetite. The magnetite powder (in 0.5-g quantities) was dissolved in 10.0-ml aliquots of TBME. The magnetite suspension was sonificated again, and any insoluble material was separated by centrifugation. The resulting clear brown suspension was stable (over a period of at least 3 months) and used as the stock solution 1 (29 g/l solid matter). The particles were stabilized by the lauric acid and had a mean size of approximately 17 nm. This corresponds with the results given in literature [17]. The shape of the particles is also shown in transmission electron microscopy (TEM) images in literature [17].

Preparation of the different test series

To measure the influence of OTS added to different solutions of stabilized iron oxide nanoparticles, we used OTS (3.88 g/l) in TBME as stock solution 2. In a series of experiments, we added different amounts of stock solutions 1 and 2 in the measuring cuvette and filled them with TBME up to a volume of 1500 μl. The resulting concentrations of magnetic particles and OTS are summarized in Table 1.

Laser light scattering measurements

The light scattering experiments (both SLS and DLS) were performed using the Zetasizer Nano instrument (Malvern). A 4-mW He–Ne laser (633 nm wavelength) with a fixed detector angle of 173° was used for the measurements. All measurements were carried out at 25 °C. About 1 ml of the dust-free sample was transferred to a special light scattering cell, and the temperature was controlled within a tolerance of ±0.02 °C. The experiments were started 10 min after the

Table 1 Concentrations of magnetic particles and OTS for different samples

Sample name	Concentration of iron oxide nanoparticles C_{mag} (g/*l*)	Concentration of OTS C_{OTS} (g/l)	C_{OTS}/C_{mag}
Series A: Constant concentration of OTS in tert-butylmethylether			
A1	3.95	0.026	0.00655
A2	1.97	0.026	0.01313
A3	0.99	0.026	0.02612
A4	0.39	0.026	0.06631
A5	0.20	0.026	0.1293
Series B: Constant concentration of magnetic nanoparticles in tert-butylmethylether			
B1	0.75	0	0
B2	0.75	0.00349	0.00465
B3	0.75	0.00698	0.00931
B4	0.75	0.01397	0.01863
B5	0.75	0.01746	0.02328
B6	0.75	0.02793	0.03724
B7	0.75	0.03685	0.04913
B8	0.75	0.06983	0.09311

sample was placed in the DLS instrument to allow the temperature to equilibrate. To obtain a reliable estimate of particle size, DLS measurements should be made within the dilute regime to avoid nonideality arising from concentration effects. These phenomena are due to interparticle interaction and multiple scattering. To reduce the interparticle interaction effects, magnetic particle samples were measured at different concentrations, and no significant size variations were observed. To reduce multiple scattering effect, noninvasive back scattering techniques were used. In this technique, the illuminating laser beam and detected scattered light need not travel through the entire sample. This reduces the chance that incident and scattered photons will encounter more than one particle, hence reducing the extent of multiple scattering. In addition, it is also possible to measure the scattered intensity at different depths within the sample. Measuring closer to the cuvette wall will reduce the effect of multiple scattering by minimizing the path length over which the scattered light has to pass. In our case, measurement positions were changed manually to record the effect of changing this parameter. Samples were measured at five different positions. The minimum position was chosen such that the detection volume was near to the cuvette wall, whereas the maximum position was located near the center of the cuvette. No significant difference of experimental data was observed as a function of varying the measuring position in the cuvette. This indicates that multiple scattering was not significant in our measurements. Therefore, for all forthcoming experiments, the measurement position was determined automatically through an optimization procedure of the signal to noise ratio of the scattered light.

Atomic force microscopy

AFM images were recorded in air at room temperature using a 100 μm 100 μm piezoelectric scan head (J-Scanner) with a multimode Digital Nanoscope IV instrument. Tapping mode and phase imaging studies were performed using a stiff silicon cantilever tip with a bending spring constant of 29–61 N/m (manufacture specified; Nanosensors Switzerland). Oscillation was performed close to its resonance frequency (302–382 kHz). The scan rate was 1 Hz, and the applied force was set at its minimum. Larger images not shown in this publication (10 μm × 10 μm) were taken to check that the smaller scaled images show typical structures. To eliminate imaging artifacts, the scan direction was systematically varied. All images were plane fit and flattened in Nanoscope IV software version 5.1.2 rb (Digital Instruments, Santa Barbara, CA) without using any filtering procedure. Dimensions of the domains were measured directly from the AFM height images. Phase imaging can provide information on heterogeneities in samples and is therefore a good complement to the topographic measurements. For the interpretation, absolute values of the phase contrast are not reliable, while relative values within an image are more accurate [18]. To characterize some small particles by AFM the particles need to be fixed onto the substrate. We achieved this by dipping the substrate into the liquid samples of magnetic nanoparticles with and without OTS [Sample B1 and B7 (aging time: 500 min)].

Acoustic spectroscopy

For these experiments, we used a DT-1200 Acoustic spectrometer developed by Dispersion Technology, New York, USA [19]. Measurements are carried out at 25 °C in a 50-ml sample cell and a frequency range of 3–100 MHz. A linear transmitter–receiver arrangement with transmission tone-burst variable gap technique is used, which was basically introduced by Andreae [20, 21]. The gap varies from close to zero up to 20 mm with precision of a few microns due to the measurements whereas 18 frequencies are chosen. Eight hundred pulses with rectangular envelope are sent through the liquid for a given frequency, but the number will be increased if the signal to noise ratio is less than 40 dB. The spectrometer measures the ultrasonic attenuation and sound speed as well and calculates the particle size distribution (PSD) from it. In general, the sound attenuation of a dispersed system is the sum of scattering and absorption. Scattering does not play a role here because it is only relevant for particles larger than 3 μm. Absorption of sound can be caused by intrinsic, viscous, thermal, and structural losses.

The viscous loss plays the major role for attenuation by small particles with high density contrast (between medium and particle) like it is the case for iron oxide. The density,

sound speed, and ultrasonic attenuation curve of both the medium and the dispersed particles must be put in the database before measurements. In comparison to the inner core the influence of the organic shell on the measured attenuation, spectra is negligible. Therefore, the acoustic spectroscopy measures only the core of the particles.

The shape of particles cannot be detected by this technique yet.

Results and discussion

Laser light scattering

In DLS experiments, the intensity time autocorrelation function $g_2(t)$ was recorded. For each sample, this function was measured fivefold. The average values of these five measurements were used for data fitting. The autocorrelation function of the scattered intensity was analyzed by means of cumulants method [22]. This method is nowadays routinely applied to analyze the DLS data for polymers and colloidal systems, and this treatment of experimental data allows determining the diffusion constant and poydisperse index (PDI). From the diffusion coefficient D_0, the so-called hydrodynamic diameter (ξ_H) can be calculated through the Stokes–Einstein relation:

$$\xi_H = \frac{k_B T}{6\pi\eta D_0} \tag{1}$$

Parameter k_B is Boltzmann's constant, T denotes the absolute temperature, and η describes the solvent viscosity. Alternatively, the data can be analyzed using the inverse Laplace transform program CONTIN [23], which better accounts for a continuous distribution of relaxation rates. However, it must be remarked that Laplace inversion method lead, in our results, to distributions of diameters that are similar to the values obtained from cumulant methods. The size distribution estimated from PDI was also consistent with the size variations obtained from CONTIN methods. Therefore, for the sake of simplicity, we present the results obtained from cumulant methods. The monomodal (cumulant) method is used to compare the results obtained from CONTIN. Sizes obtained from those methods are intensity (z-average) values.

As shown in Figs. 2b and 3b, PDI $\gamma = \frac{\langle R_h^2 \rangle}{\langle R_h \rangle^2} - 1$ measured for all systems is 0.05–0.20 with an error ±10%. This suggests that the stable suspensions have reasonably narrow size distributions.

OTS concentration effect Different concentrations of OTS were injected into solutions keeping constant concentration of iron oxide nanoparticles. All different concentrations, used in these experiments, are listed in Table 1. Typical results are represented in Fig. 1. Comparing the curves of different OTS concentrations in Fig. 1, it is evident that OTS molecules start depositing on iron oxide nanoparticles above a certain concentration. Under conditions where this threshold concentration was exceeded, the size of coated iron oxide nanoparticles increased rapidly at the initial stages of the process. However, adsorption of OTS continued for long periods of time at reduced rates before reaching a final plateau value. Further increase of OTS concentration above a certain value destabilized the system, and phase separation occurred. It can be seen in Fig. 1a and b that for

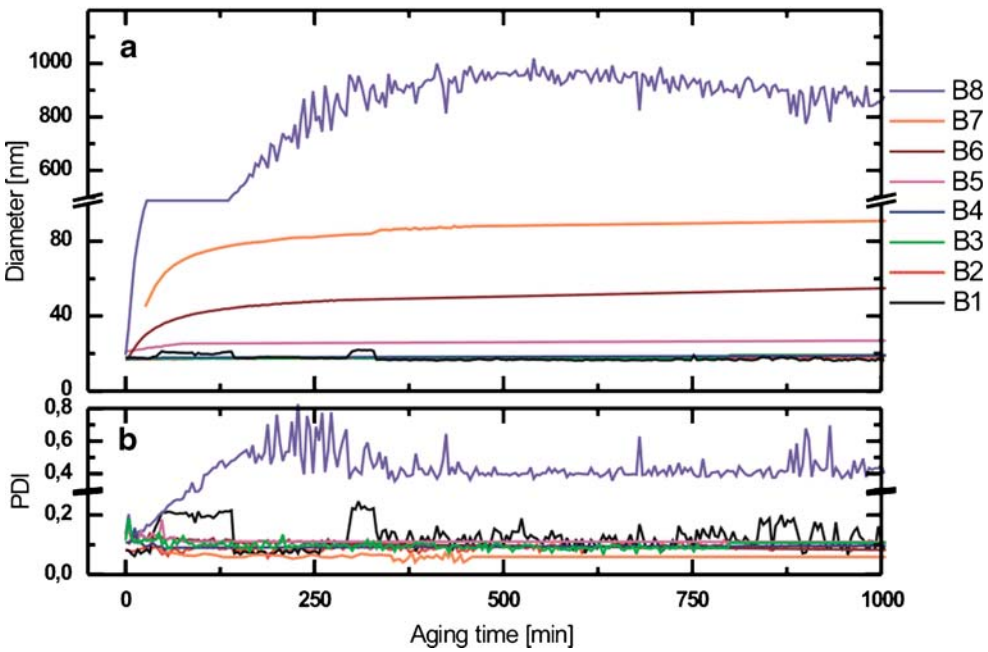

Fig. 1 (**a**) Aging time vs hydrodynamic diameter of OTS coated iron oxide nanoparticles obtained from DLS. (**b**) PDI as a function of aging time of OTS-coated magnetic particles. Errors are smaller than ±2% for the diameter and ±10% for the PDI. The different probes B1–B8 are described in Table 1

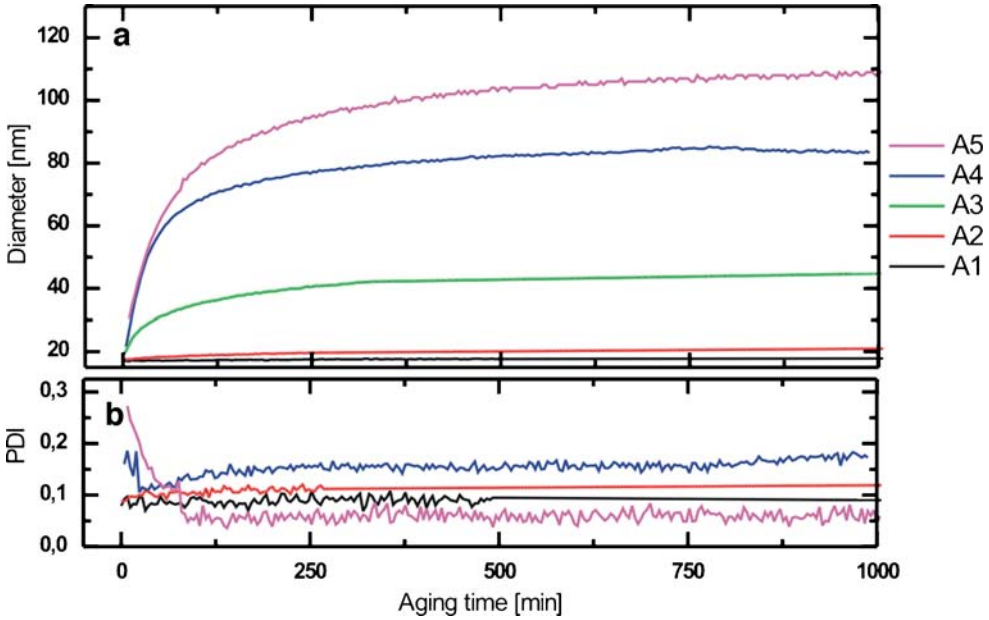

Fig. 2 (**a**) Hydrodynamic diameter vs aging time of OTS-coated magnetic nanoparticles obtained from DLS. (**b**) PDI vs aging time of OTS-coated magnetic particles. Errors are smaller than ±2% for the diameter and ±10% for the PDI. The different probes A1–A5 are described in Table 1

system B8, size and polydispersity increased very fast. It turned out that the diameter reached values of the micrometer range in a few hours, leading to unstable suspensions. It can also be seen in Fig. 1 that for a given concentration of iron oxide nanoparticles, increased OTS concentration results in higher rates of particle growth.

Iron oxide concentration effect The different concentrations of iron oxide were injected into solution keeping constant concentration of OTS (see Table 1). The results are summarized in Fig. 2.

As can be seen in Fig. 2, similar behavior mentioned above is observed for the variation of concentration of iron oxide nanoparticles. Figures 1 and 2 suggest that the size of OTS-coated iron oxide nanoparticles is dominantly characterized by the concentration ratio μ rather than actual concentration.

Particle growth as a function of the concentration relationship μ Plateau size values of OTS-coated iron oxide nanoparticles vs μ are plotted in Fig. 3. Below a critical ratio $\mu<0.02$, we did not observe any significant increase in the nanoparticle size. Above this threshold value, the particle diameter increased rapidly and followed second-order polynomial behavior.

The particles are probably not uniform spherical as shown schematically in Fig. 3. The shape of the primary magnetite particles is shown by TEM in literature [17].

As shown in Figs. 1 and 2, the particle growth rate increased for elevated values of the concentration ratio μ at the initial stage of the process.

As shown in Fig. 4, a similar effect as obtained for hydrodynamic size can be observed in the dependence of the scattered intensity on aging time. Above the threshold value of μ, scattering intensity increased rapidly at the initial stages of the process and continued to grow for long periods of time at reduced rates before finally reaching a plateau value. For the unstable system B8, the scattering intensity increased very fast and then started decreasing. Decreasing scattered intensity indicated a precipitation of iron oxide nanoparticles.

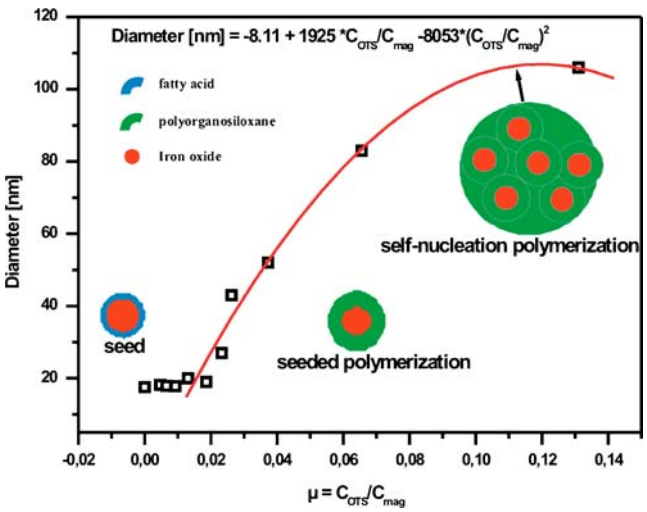

Fig. 3 Variation in magnetic nanoparticle size as a function of the concentration ratio of OTS and uncoated magnetic nanoparticles (C_{OTS}/C_{mag}). Possible growth mechanism are also shown (see text for details and schematic is not drawn to the scale)

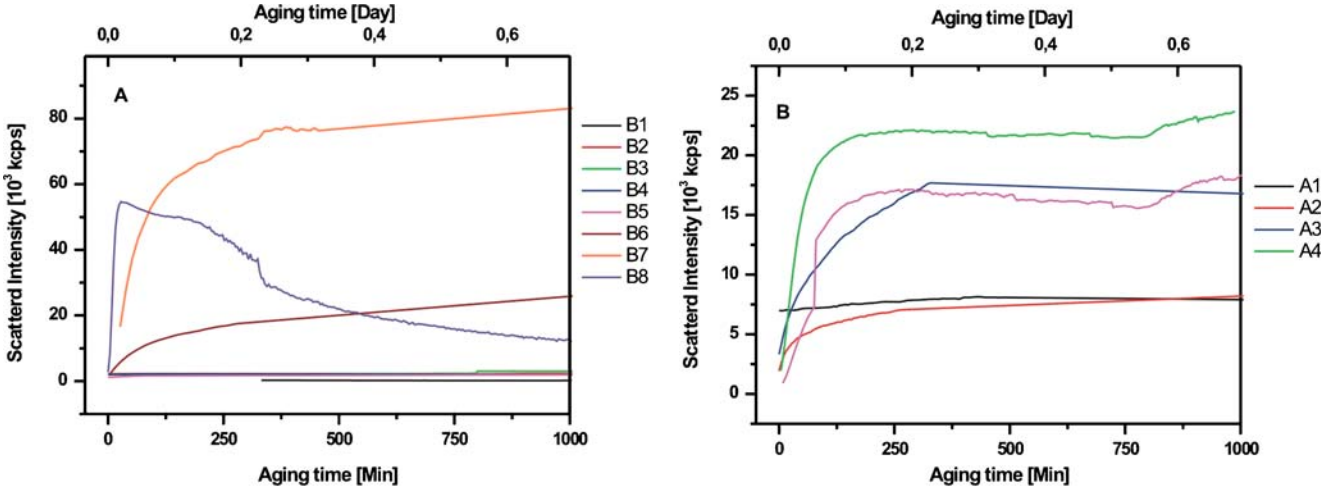

Fig. 4 Scattered intensity versus aging time of OTS-coated magnetic nanoparticles obtained from SLS. (**a**) Keeping constant magnetic particles and varying the amount of OTS. (**b**) Varying the amount of magnetic particles and keeping constant the amount of OTS

In a series of SLS experiments, we measured the time-average (or 'total') intensity of the scattered light. This signal arises from concentration fluctuation of the particles in solution. The excess scattering intensity I of the particles over that of the continuous phase is described by [22]:

$$I \approx \frac{4\pi R^3 G}{3}\left(\frac{\partial n}{\partial \phi}\right)^2 (1 + B\phi)^{-1} \qquad (2)$$

In this study, G is a constant characteristic of the instrument, n is the refractive index of the solution, R denotes the particle size, ϕ describes the volume fraction of particles, and B is the second virial coefficient. If the systems under study are ideal, mixtures $\left(\frac{\partial n}{\partial \phi}\right)$ is constant, and B is then negligible. Under these conditions, the scattering intensity should be a function of R^3 provided ϕ also remains constant. As we did not observe a significant concentration dependence of the investigated nanoparticles, we can assume that B is small. Under these conditions, the scattering intensity should follow Eq. 2. In Fig. 5, we demonstrate that the scattered intensity follows the ideal R^3 behavior. The data, obtained from DLS and SLS experiments are, hence, in good agreement.

Atomic force microscopy

Tapping mode along with phase imaging techniques of AFM were used to analyze the samples B1 and B7 (aging time, 500 min). The samples were prepared on a silicon wafer using a dipping process. The AFM imaging was performed just to confirm the dimensions of the iron oxide nanoparticles and to investigate the influence of OTS molecules on the shape and size. Figure 6a,b and c present AFM heights and phase images as well as their sizes from section analysis for the sample B7. Similar measurements were performed for system B1 (AFM images are not shown). The results of these experiments point to distinct differences between OTS-coated and noncoated iron oxide nanoparticles. In case of iron oxide nanoparticles coated by OTS, cluster of iron cores were embedded in an OTS shell. This can be easily seen in the phase image (Fig. 6b). The solid black line is encircling the white cluster of iron cores (~40 nm). The red dotted line surrounding the light brownish part corresponds to the OTS shell (~7 nm). This indicates that OTS-coated nanoparticles (B7) have sizes of about 54 nm. This result is consistent with DLS result (~90 nm) for the same sample B7. The hydrodynamic particle diameter measured by DLS is larger than the static core measured by AFM because it includes attached layers of solvents, which migrate with the particles.

In the phase imaging Fig. 6b, nanoparticles can be seen as separated spots (e.g., white spot inside the red circles)

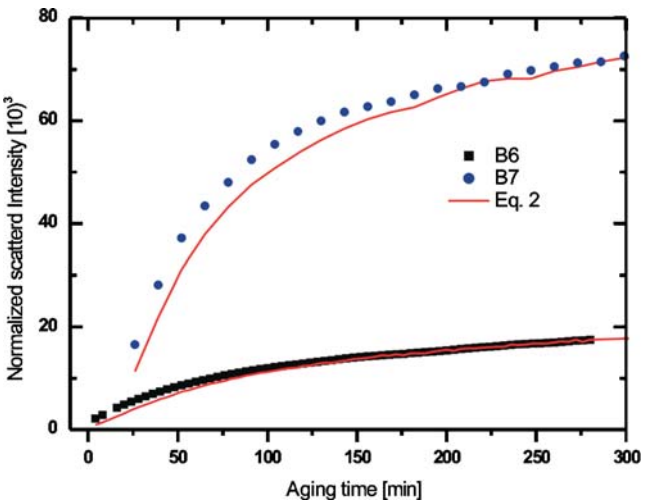

Fig. 5 Normalized scattering intensity as the function of time. The *solid lines* are the predictions according to Eq. 2

with diameters in the range from 8.8 to 23 nm. This is in very good agreement with the particle sizes of the pure iron oxide particles (without OTS) measured by DLS (~16 nm). The iron oxide nanoparticles are embedded in the OTS matrix, which can also be seen in the height image (Fig. 6a). As shown in Fig. 6c, a cross-section along a line marked in Fig. 6a gives a height of the embedded magnetic particles of approximately 16 nm. The height of the surrounded OTS matrix is approximately 7 nm. These values are consistent with the data obtained from phase images and DLS measurements. The formation of single clusters as seen in Fig. 6b could be caused by the agglomeration process discussed above. Another reason could be the transfer of the particles on the surface. During evaporation of the liquid, a precipitation process could occur. This can also explain the observed aggregates but could not be the reason for the increasing values in the particle diameter by DLS measurements.

Acoustic spectroscopy

An acoustic spectrometer does not directly measure particle size similar to alternate method like light scattering. It measures an attenuation spectrum and calculates the particle size assuming a certain model for describing the sound attenuation in terms of the physical properties of the system. Similar to AFM, we investigated sample B1 using acoustic spectroscopy. The attenuation was measured over a frequency range from 3 to 100 MHz. As shown in Fig. 7a, measurements

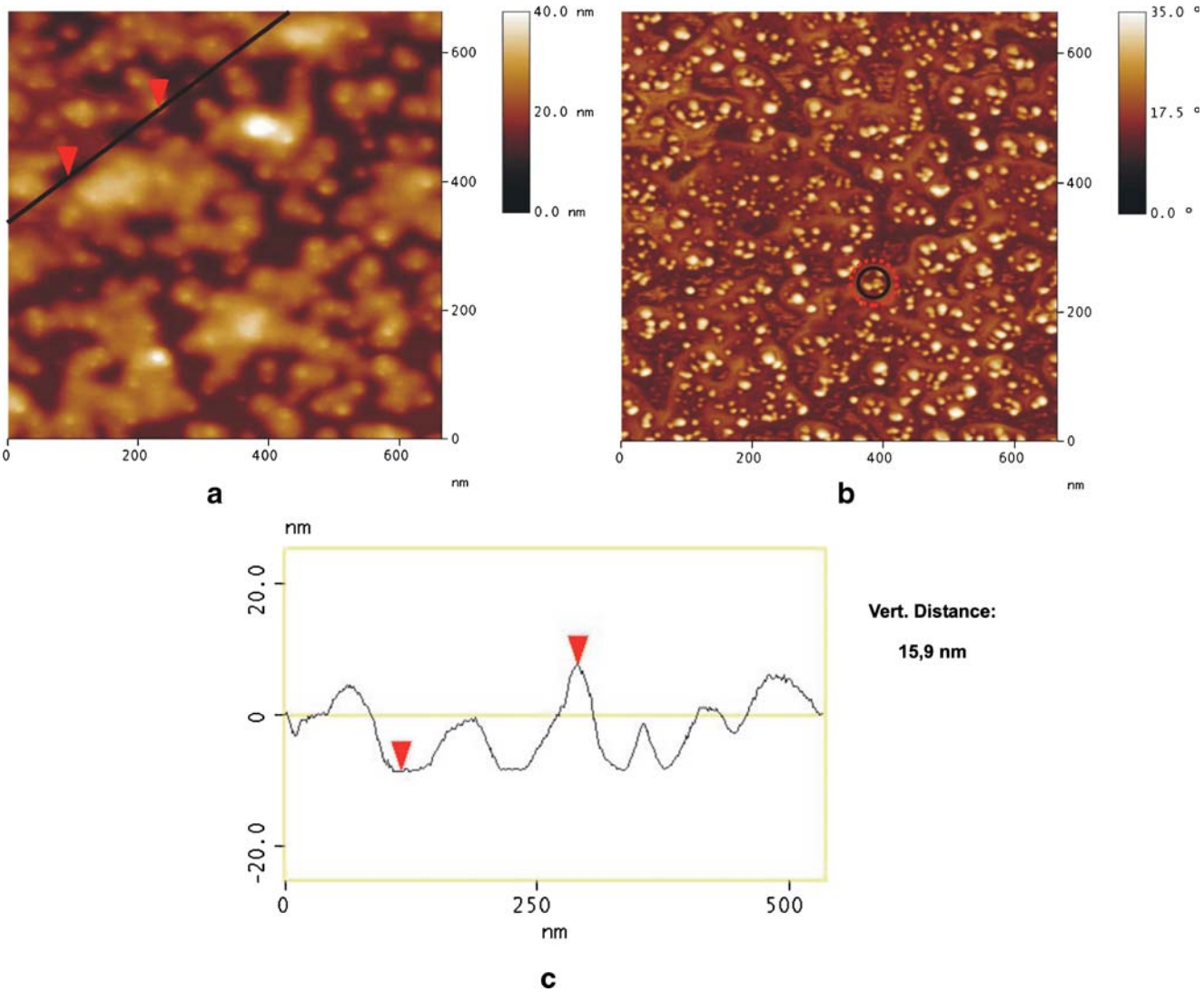

Fig. 6 Magnetic nanoparticles embedded in an OTS shell and transferred on a silicon wafer (sample B7): (**a**) tapping mode AFM (the *shaded bar* is a measure of height); (**b**) phase imaging AFM (the *shaded bar* is a measure of phase angle); (**c**) A cross section along the line indicated in (**a**). The vertical distance is measured between the two marked points

were repeated five times. The good reproducibility showed by this test indicated that the sample stability and good instrument performance.

Some experimental points at low frequency (<7 MHz) and at high frequency (>50 MHz) are excluded because of the large errors. (Those frequencies were in the vicinities of the transducer piezocrystal harmonics). The monomodal hypothesis is used to fit experimental attenuation curves [24]. We assume that the size distribution can be properly described by a log-normal distribution. The corresponding log-normal PSD is shown in Fig. 7b. The mean size (D_{mean}) of the log-normal distribution in 8.6 nm, and the PDI is 0.11. Herrmann and Lemarechal [25] showed that D_{mean} extracted from the acoustic spectroscopy using log-normal distribution is related to the apparent hydrodynamic diameter ξ_{H} as

$$\xi_H D_{mean}(1+\gamma)^2 \tag{3}$$

In the formula 3, diameter obtained from acoustic spectroscopy (D_{mean}) is the volume average value, while the diameter extracted from the DLS (ξ_{H}) is intensity average (z-average). In general, the intensity average value is greater than the volume average value. The apparent hydrodynamic diameter ξ_{H} calculated using Eq. 3 with the values of D_{mean} and γ deduced from acoustic spectroscopy, is also shown in Fig. 6b. The agreement of ξ_{H} and PDI from acoustic spectroscopy with the experimental results obtained from DLS and AFM is quite good (see Fig. 6b). The slightly smaller size observed from the acoustic spectroscopy may be due to the fact that acoustic spectroscopy measure only the core of the particles.

Proposed mechanism of particle growth

By considering the growth rate, morphology, and size of the composite particles under different experimental conditions, two different mechanisms are proposed in analogy to investigations of previous scientists [26]: Mechanism I, seeded particle growth, and mechanism II, self-nucleation particle growth.

In mechanism I, when μ>0.02, the seeded particle growth started, because the surfactant film at the surface of the iron oxide nanoparticles absorbed OTS monomers and polymerization occurred (Influence of water). Some free Fe–OH groups may have participated in the adsorption

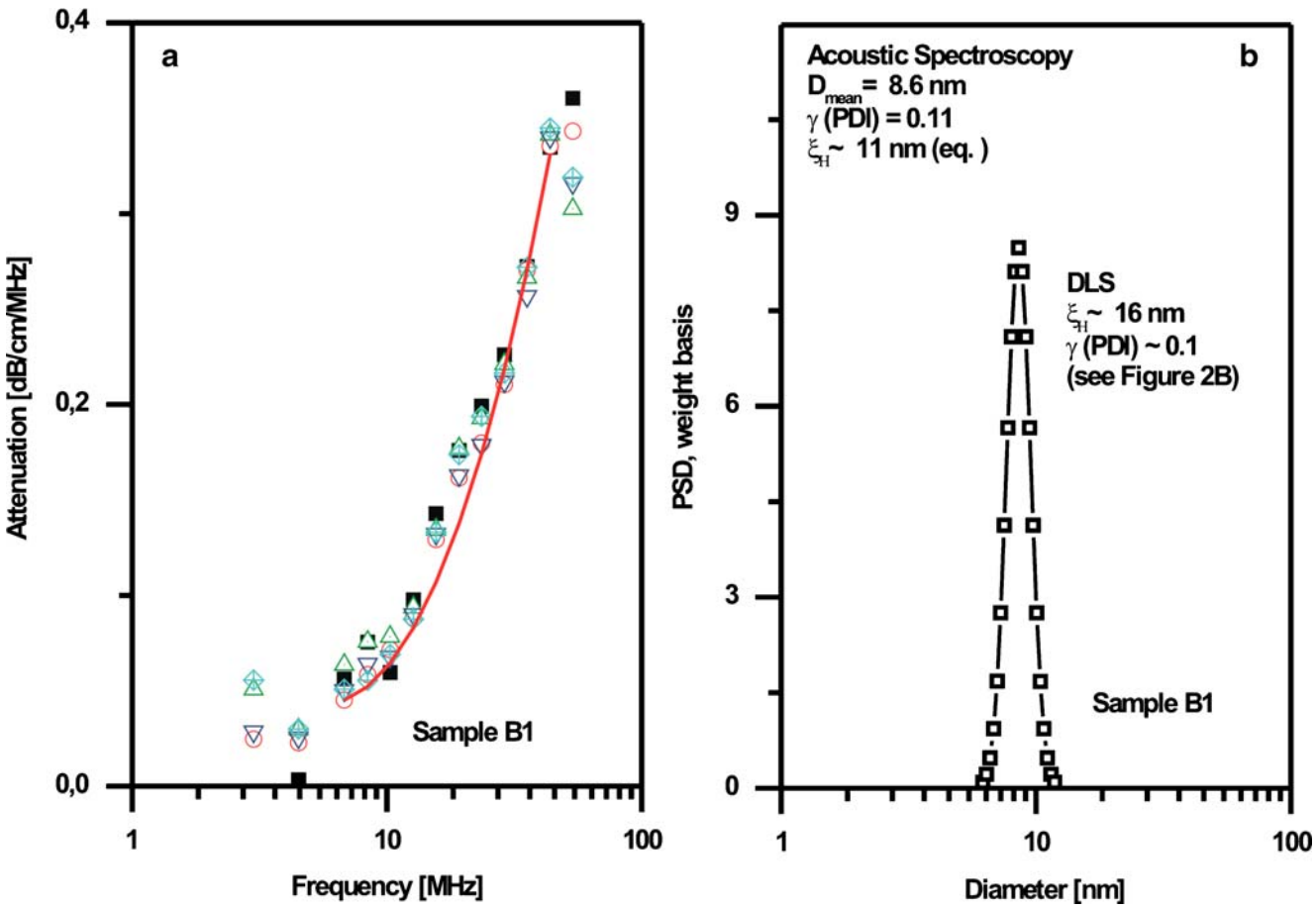

Fig. 7 (**a**) Experimental (five measurements: *symbols*) and theoretical (*red solid line*) attenuation spectra for sample B1. (**b**) Log-normal PSD extracted from attenuation spectra

of OTS at iron oxide nanoparticle surface [12]. This is consistent with the observed (6 nm) increase in radius of iron oxide nanoparticles (DLS) just above the critical threshold concentration ratio μ.

In mechanism II, at elevated OTS concentrations, the surfactant layer may be destroyed by the large amount of excess OTS molecules. Under these conditions, significant coagulation of iron oxide nanoparticles occurred, and the particle growth proceeded mostly through self-nucleation. Iron oxide nanoparticles coagulated with each other until a new stability was regained by adsorption of OTS molecules. Particle growth is generally faster in case of self-nucleation than in seeded polymerization [25]. This is consistent with the observed cluster of iron oxide nanoparticles (~40 nm: B7) in OTS shell (~7 nm) for OTS-rich sample B7 from AFM.

As mentioned above, Figs. 2 and 3 show the particle growth at different stages of aging. These figures indicated that at higher monomer concentrations (large values of μ), the particle size and the rate of particle growth increased. For samples of series A, particle growth started from sample A3, and for series B, particle growth was observed from sample B5. The particle sizes slowly increased up to about 27 nm for sample B5. This suggests that the coated iron oxide nanoparticles of sample B5 were modified by adsorption and cross-linking of OTS molecules around the iron oxide nanoparticles. In the case of the A3 samples, more monomer was present, and the particle size was larger than B5 as expected. This suggests that the surfactant layer was destroyed due to the presence of excess OTS molecules. This favors coagulation until a new stability was regained by the adsorption of OTS molecules at the iron oxide surface. Thus, the stable OTS-coated iron oxide nanoparticles were mainly generated from seeded particle growth and partially from self-nucleation. Coagulation of seed particles increased with the increase in μ. We first measured a marked growing process in the particle size of B8, and after some time, the system became unstable, and one could observe the precipitation. This could be explained by the fact that B8 samples have high nanoparticles and monomer concentrations. Both factors favor the coagulation of iron oxide nanoparticles: at elevated concentration, the particle coagulation occurred more frequently, and excess monomer destroyed the surfactant layers. For the B8 samples, the coated iron oxide nanoparticles were mainly generated through self-nucleation, which made them unstable.

Figure 8 shows the surface area per OTS molecule calculated from elementary analysis. These measurements (See Fig. 8) reconfirmed the above-mentioned mechanism for particle growth. It turns out that the size of the coated iron oxide nanoparticles is correlated with the amount of OTS. As shown in Fig. 8, for μ>0.050, surface area

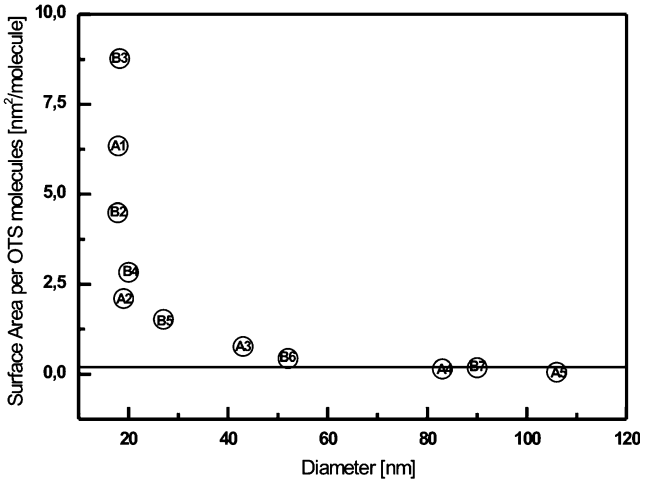

Fig. 8 Surface area per OTS molecule as a function of the nanoparticles size. The reported values were obtained after subtraction of the monolayer shell of OTS from measured plateau values. The *solid line* describes the required surface area for each bonded molecule, which is needed to form close-packed monolayer coverage [21]

occupied by OTS molecules is of the order of 0.2 nm^2. This corresponds well with the literature values for formation of close-packed monolayer coverages [24]. It is interesting, to note, that a certain minimum surface concentration 1.52 nm^2 per reactive monomer of OTS is required for the particle growth. Similar threshold concentrations were observed for the formation of two-dimensional networks at the oil–water interface [24].

In our laboratory, we do not have the facility to measure the magnetic behavior of the nanoparticles in detail (for example by B–H curves). Therefore, we could not predict the magnetic behavior of the nanoparticles after polymerization process. But we are sure that in both, the polymer coated particles and the noncoated ones, the inner core is magnetic. Both liquid suspensions showed macroscopic reaction on an outer magnetic field in a range of approximately 0.1 T.

Conclusions

In a series of experiments, we used light scattering, acoustic spectroscopy, and AFM measurements to explore the SA coating of OTS at the surface of iron oxide nanoparticles. The results of these different experiments were found to be in fairly good agreement. We observed that DLS and SLS are powerful techniques to characterize such type of nanoparticles especially in the regime of relatively low concentrations. In contrast to other methods that provide similar information, light scattering technique is relatively quick and reproducible and does not require calibration standards or complicated sample preparations.

In a series of experiments, we observed that the size growth rate and the final diameter was highly dependent on

the concentration ratio $\mu = C_{OTS}/C_{mag}$. In conclusion, uniform, OTS-coated iron oxide nanoparticles have been synthesized in the range from 27 to 100 nm with narrow size distribution. The results of our experiments showed that two different mechanisms of particle growth were involved depending on the different values of μ. In the regime of low OTS concentrations (small values of μ), seeded polymerization was the main source to form OTS-coated nanoparticles. In regions of excess OTS concentrations (large values of μ), coagulation processes occurred before regaining stability. In this concentration regime, we therefore, observed the formation of large aggregates.

References

1. Rao CNR, Müller A, Cheetham AK (eds) (2004) The chemistry of nanomaterials: synthesis, properties and application. Wiley, Weinheim
2. Ulman A (1991) An introduction to ultrathin organic films: from langinuir-blodgett to self-assembly. Academic, Boston
3. Ulman A (1996) Chem Rev 96:1533
4. Bascom WDJ (1968) Colloid Interface Sci 26:89
5. Nainyong KY, Laibinis PE (1997) J Am Chem Soc 119:2297
6. Nuzzo RG, Allara DL (1983) J Am Chem Soc 105:4481
7. Sandorff CJ, Garoff S, Leung KP (1983) Chem Phys Lett 96:547
8. Laibinis PE, Whiteside GM, Allara DL, Tao Y-T, Parikh AN, Nuzzo RG (1991) J Am Chem Soc 113:7152
9. Ulman A, Evans SD, Shnidman Y, Sharma R, Eilers J-E, Chang JC (1991) J Am Chem Soc 113:1499
10. Kataby G, Ulman A, Prozorov R, Gedanken A (1998) Langmuir 14:1512
11. Kataby G, Cojocaru M, Prozorov R, Gedankeri A (1999) Langmuir 15:1703
12. Rozenfeld O, Koltypin Y, Bamnolker H, Margel S, Gedanken A (1994) Langmuir 10:627
13. Shukla A, Degen P, Rehage H (2007) J Am Chem Soc 29(26):8056
14. Binning G, Quate CF, Gerber C (1986) Phys Rev Lett 56:930
15. Chernoff DA (1995) Proc Microsc Microanal 888
16. Chernoff DA (1996) Nanocations Winter 1996. Digital Instruments, Santa Barbara, CA, p 6
17. Meldrum FC, Kotov NA, Fendler JH (1994) J Phys Chem 98:4506–4510
18. Overney RM, Meyer E, Frommer J, Güntherodt H-J (1994) Langmuir 10:1281
19. Dukhin AS, Goetz PJ (1998) Colloids Surf 144:49
20. Koppel DE (1972) J Chem Phys 57:4814
21. Provencher SW (1982) Comput Phys Commun 27:229
22. Cazabat AM, Langevin D (1981) J Chem Phys 74:3148
23. Herrmann N, Lemarechal P (1999) Eur Phys J AP 5:127
24. Rehage H, Achenbach B, Husmann M (1999) Ultrathin cross-linked polyorganosiloxane networks at interfaces between fluids: structure, properties and preparative prospectives. In: Stokke BT, Elgsaeter A (eds) The Wiley polymer network review series, 2nd edn. Wiley, Chichester, Weinheim, New York, pp 444–459
25. Wang PC, Chiu WY, Lee CF, Young TH (2004) J Poly Sci A 42:5695
26. Wasserman SR, Tao YT, Whitesides GM (1989) Langmuir 5:1074